



First observation of the decay $B_{s2}^{*0}(5840) \rightarrow B^{*+}K^{-}$ and studies of excited B_s^0 mesons

The LHCb collaboration[†]

Abstract

Properties of the orbitally excited ($L = 1$) B_s^0 states are studied using 1.0 fb^{-1} of pp collisions at $\sqrt{s} = 7 \text{ TeV}$ collected with the LHCb detector. The first observation of the $B_{s2}^{*0}(5840)$ meson decaying to $B^{*+}K^{-}$ is reported, and the corresponding branching fraction measured relative to the B^+K^{-} decay mode. The $B_{s1}(5830)^0 \rightarrow B^{*+}K^{-}$ decay is observed as well. The width of the $B_{s2}^{*0}(5840)$ state is measured for the first time and the masses of the two states are determined with the highest precision to date. The observation of the $B_{s2}^{*0}(5840) \rightarrow B^{*+}K^{-}$ decay favours the spin-parity assignment $J^P = 2^+$ for the $B_{s2}^{*0}(5840)$ meson. In addition, the most precise measurement of the mass difference $m(B^{*+}) - m(B^+) = 45.01 \pm 0.30 \text{ (stat)} \pm 0.23 \text{ (syst)} \text{ MeV}/c^2$ is obtained.

Submitted to Phys. Rev. Lett.

[†]Authors are listed on the following pages.

LHCb collaboration

R. Aaij³⁸, C. Abellan Beteta^{33,n}, A. Adametz¹¹, B. Adeva³⁴, M. Adinolfi⁴³, C. Adrover⁶, A. Affolder⁴⁹, Z. Ajaltouni⁵, J. Albrecht³⁵, F. Alessio³⁵, M. Alexander⁴⁸, S. Ali³⁸, G. Alkhazov²⁷, P. Alvarez Cartelle³⁴, A.A. Alves Jr^{22,35}, S. Amato², Y. Amhis³⁶, L. Anderlini^{17,f}, J. Anderson³⁷, R.B. Appleby⁵¹, O. Aquines Gutierrez¹⁰, F. Archilli¹⁸, A. Artamonov³², M. Artuso⁵³, E. Aslanides⁶, G. Auriemma^{22,m}, S. Bachmann¹¹, J.J. Back⁴⁵, C. Baesso⁵⁴, V. Balagura²⁸, W. Baldini¹⁶, R.J. Barlow⁵¹, C. Barschel³⁵, S. Barsuk⁷, W. Barter⁴⁴, A. Bates⁴⁸, Th. Bauer³⁸, A. Bay³⁶, J. Beddow⁴⁸, I. Bediaga¹, S. Belogurov²⁸, K. Belous³², I. Belyaev²⁸, E. Ben-Haim⁸, M. Benayoun⁸, G. Bencivenni¹⁸, S. Benson⁴⁷, J. Benton⁴³, A. Berezhnoy²⁹, R. Bernet³⁷, M.-O. Bettler⁴⁴, M. van Beuzekom³⁸, A. Bien¹¹, S. Bifani¹², T. Bird⁵¹, A. Bizzeti^{17,h}, P.M. Bjørnstad⁵¹, T. Blake³⁵, F. Blanc³⁶, C. Blanks⁵⁰, J. Blouw¹¹, S. Blusk⁵³, A. Bobrov³¹, V. Bocci²², A. Bondar³¹, N. Bondar²⁷, W. Bonivento¹⁵, S. Borghi⁵¹, A. Borgia⁵³, T.J.V. Bowcock⁴⁹, C. Bozzi¹⁶, T. Brambach⁹, J. van den Brand³⁹, J. Bressieux³⁶, D. Brett⁵¹, M. Britsch¹⁰, T. Britton⁵³, N.H. Brook⁴³, H. Brown⁴⁹, A. Büchler-Germann³⁷, I. Burducea²⁶, A. Bursche³⁷, J. Buytaert³⁵, S. Cadeddu¹⁵, O. Callot⁷, M. Calvi^{20,j}, M. Calvo Gomez^{33,n}, A. Camboni³³, P. Campana^{18,35}, A. Carbone^{14,c}, G. Carboni^{21,k}, R. Cardinale^{19,i}, A. Cardini¹⁵, H. Carranza-Mejia⁴⁷, L. Carson⁵⁰, K. Carvalho Akiba², G. Casse⁴⁹, M. Cattaneo³⁵, Ch. Cauet⁹, M. Charles⁵², Ph. Charpentier³⁵, P. Chen^{3,36}, N. Chiapolini³⁷, M. Chrzaszcz²³, K. Ciba³⁵, X. Cid Vidal³⁴, G. Ciezarek⁵⁰, P.E.L. Clarke⁴⁷, M. Clemencic³⁵, H.V. Cliff⁴⁴, J. Closier³⁵, C. Coca²⁶, V. Coco³⁸, J. Cogan⁶, E. Cogneras⁵, P. Collins³⁵, A. Comerma-Montells³³, A. Contu¹⁵, A. Cook⁴³, M. Coombes⁴³, G. Corti³⁵, B. Couturier³⁵, G.A. Cowan³⁶, D.C. Craik⁴⁵, S. Cunliffe⁵⁰, R. Currie⁴⁷, C. D'Ambrosio³⁵, P. David⁸, P.N.Y. David³⁸, I. De Bonis⁴, K. De Bruyn³⁸, S. De Capua⁵¹, M. De Cian³⁷, J.M. De Miranda¹, L. De Paula², P. De Simone¹⁸, D. Decamp⁴, M. Deckenhoff⁹, H. Degaudenzi^{36,35}, L. Del Buono⁸, C. Deplano¹⁵, D. Derkach¹⁴, O. Deschamps⁵, F. Dettori³⁹, A. Di Canto¹¹, J. Dickens⁴⁴, H. Dijkstra³⁵, P. Diniz Batista¹, M. Dogaru²⁶, F. Domingo Bonal^{33,n}, S. Donleavy⁴⁹, F. Dordei¹¹, A. Dosil Suárez³⁴, D. Dossett⁴⁵, A. Dovbnya⁴⁰, F. Dupertuis³⁶, R. Dzhelyadin³², A. Dziurda²³, A. Dzyuba²⁷, S. Easo^{46,35}, U. Egede⁵⁰, V. Egorychev²⁸, S. Eidelman³¹, D. van Eijk³⁸, S. Eisenhardt⁴⁷, U. Eitschberger⁹, R. Ekelhof⁹, L. Eklund^{48,35}, I. El Rifai⁵, Ch. Elsasser³⁷, D. Elsby⁴², A. Falabella^{14,e}, C. Färber¹¹, G. Fardell⁴⁷, C. Farinelli³⁸, S. Farry¹², V. Fave³⁶, D. Ferguson⁴⁷, V. Fernandez Albor³⁴, F. Ferreira Rodrigues¹, M. Ferro-Luzzi³⁵, S. Filippov³⁰, M. Fiore¹⁶, C. Fitzpatrick³⁵, M. Fontana¹⁰, F. Fontanelli^{19,i}, R. Forty³⁵, O. Francisco², M. Frank³⁵, C. Frei³⁵, M. Frosini^{17,f}, S. Furcas²⁰, A. Gallas Torreira³⁴, D. Galli^{14,c}, M. Gandelman², P. Gandini⁵², Y. Gao³, J.-C. Garnier³⁵, J. Garofoli⁵³, P. Garosi⁵¹, J. Garra Tico⁴⁴, L. Garrido³³, C. Gaspar³⁵, R. Gauld⁵², E. Gersabeck¹¹, M. Gersabeck³⁵, T. Gershon^{45,35}, Ph. Ghez⁴, V. Gibson⁴⁴, V.V. Gligorov³⁵, C. Göbel⁵⁴, D. Golubkov²⁸, A. Golutvin^{50,28,35}, A. Gomes², H. Gordon⁵², M. Grabalosa Gándara⁵, R. Graciani Diaz³³, L.A. Granado Cardoso³⁵, E. Graugés³³, G. Graziani¹⁷, A. Greco²⁶, E. Greening⁵², S. Gregson⁴⁴, O. Grünberg⁵⁵, B. Gui⁵³, E. Gushchin³⁰, Yu. Guz^{32,35}, T. Gys³⁵, C. Hadjivasiliou⁵³, G. Haefeli³⁶, C. Haen³⁵, S.C. Haines⁴⁴, S. Hall⁵⁰, T. Hampson⁴³, S. Hansmann-Menzemer¹¹, N. Harnew⁵², S.T. Harnew⁴³, J. Harrison⁵¹, P.F. Harrison⁴⁵, T. Hartmann⁵⁵, J. He⁷, V. Heijne³⁸, K. Hennessy⁴⁹, P. Henrard⁵, J.A. Hernando Morata³⁴, E. van Herwijnen³⁵, E. Hicks⁴⁹, D. Hill⁵², M. Hoballah⁵, P. Hopchev⁴, W. Hulsbergen³⁸, P. Hunt⁵², T. Huse⁴⁹, N. Hussain⁵², D. Hutchcroft⁴⁹, D. Hynds⁴⁸, V. Iakovenko⁴¹, P. Ilten¹², J. Imong⁴³, R. Jacobsson³⁵,

A. Jaeger¹¹, M. Jahjah Hussein⁵, E. Jans³⁸, F. Jansen³⁸, P. Jatou³⁶, B. Jean-Marie⁷, F. Jing³,
 M. John⁵², D. Johnson⁵², C.R. Jones⁴⁴, B. Jost³⁵, M. Kaballo⁹, S. Kandybei⁴⁰, M. Karacson³⁵,
 T.M. Karbach³⁵, I.R. Kenyon⁴², U. Kerzel³⁵, T. Ketel³⁹, A. Keune³⁶, B. Khanji²⁰, Y.M. Kim⁴⁷,
 O. Kochebina⁷, I. Komarov³⁶, R.F. Koopman³⁹, P. Koppenburg³⁸, M. Korolev²⁹,
 A. Kozlinskiy³⁸, L. Kravchuk³⁰, K. Kreplin¹¹, M. Kreps⁴⁵, G. Krocker¹¹, P. Krokovny³¹,
 F. Kruse⁹, M. Kucharczyk^{20,23,j}, V. Kudryavtsev³¹, T. Kvaratskheliya^{28,35}, V.N. La Thi³⁶,
 D. Lacarrere³⁵, G. Lafferty⁵¹, A. Lai¹⁵, D. Lambert⁴⁷, R.W. Lambert³⁹, E. Lanciotti³⁵,
 G. Lanfranchi^{18,35}, C. Langenbruch³⁵, T. Latham⁴⁵, C. Lazzeroni⁴², R. Le Gac⁶,
 J. van Leerdam³⁸, J.-P. Lees⁴, R. Lefèvre⁵, A. Leflat²⁹, J. Lefrançois⁷, O. Leroy⁶, Y. Li³,
 L. Li Gioi⁵, M. Liles⁴⁹, R. Lindner³⁵, C. Linn¹¹, B. Liu³, G. Liu³⁵, J. von Loeben²⁰,
 J.H. Lopes², E. Lopez Asamar³³, N. Lopez-March³⁶, H. Lu³, J. Luisier³⁶, H. Luo⁴⁷,
 A. Mac Raighne⁴⁸, F. Machefert⁷, I.V. Machikhiliyan^{4,28}, F. Maciuc²⁶, O. Maev^{27,35},
 S. Malde⁵², G. Manca^{15,d}, G. Mancinelli⁶, N. Mangiafave⁴⁴, U. Marconi¹⁴, R. Märki³⁶,
 J. Marks¹¹, G. Martellotti²², A. Martens⁸, L. Martin⁵², A. Martín Sánchez⁷, M. Martinelli³⁸,
 D. Martinez Santos³⁹, D. Martins Tostes², A. Massafferri¹, R. Matev³⁵, Z. Mathe³⁵,
 C. Matteuzzi²⁰, M. Matveev²⁷, E. Maurice⁶, A. Mazurov^{16,30,35,e}, J. McCarthy⁴²,
 G. McGregor⁵¹, R. McNulty¹², F. Meier⁹, M. Meissner¹¹, M. Merk³⁸, J. Merkel⁹,
 D.A. Milanes¹³, M.-N. Minard⁴, J. Molina Rodriguez⁵⁴, S. Monteil⁵, D. Moran⁵¹,
 P. Morawski²³, R. Mountain⁵³, I. Mous³⁸, F. Muheim⁴⁷, K. Müller³⁷, R. Muresan²⁶,
 B. Muryn²⁴, B. Muster³⁶, J. Mylroie-Smith⁴⁹, P. Naik⁴³, T. Nakada³⁶, R. Nandakumar⁴⁶,
 I. Nasteva¹, M. Needham⁴⁷, N. Neufeld³⁵, A.D. Nguyen³⁶, T.D. Nguyen³⁶, C. Nguyen-Mau^{36,o},
 M. Nicol⁷, V. Niess⁵, R. Niet⁹, N. Nikitin²⁹, T. Nikodem¹¹, A. Nomerotski⁵², A. Novoselov³²,
 A. Oblakowska-Mucha²⁴, V. Obraztsov³², S. Oggero³⁸, S. Ogilvy⁴⁸, O. Okhrimenko⁴¹,
 R. Oldeman^{15,d}, M. Orlandea²⁶, J.M. Otalora Goicochea², P. Owen⁵⁰, B.K. Pal⁵³,
 A. Palano^{13,b}, M. Palutan¹⁸, J. Panman³⁵, A. Papanestis⁴⁶, M. Pappagallo⁴⁸, C. Parkes⁵¹,
 C.J. Parkinson⁵⁰, G. Passaleva¹⁷, G.D. Patel⁴⁹, M. Patel⁵⁰, G.N. Patrick⁴⁶, C. Patrignani^{19,i},
 C. Pavel-Nicorescu²⁶, A. Pazos Alvarez³⁴, A. Pellegrino³⁸, G. Penso^{22,l}, M. Pepe Altarelli³⁵,
 S. Perazzini^{14,c}, D.L. Perego^{20,j}, E. Perez Trigo³⁴, A. Pérez-Calero Yzquierdo³³, P. Perret⁵,
 M. Perrin-Terrin⁶, G. Pessina²⁰, K. Petridis⁵⁰, A. Petrolini^{19,i}, A. Phan⁵³,
 E. Picatoste Olloqui³³, B. Pie Valls³³, B. Pietrzyk⁴, T. Pilar⁴⁵, D. Pinci²², S. Playfer⁴⁷,
 M. Plo Casasus³⁴, F. Polci⁸, G. Polok²³, A. Poluektov^{45,31}, E. Polycarpo², D. Popov¹⁰,
 B. Popovici²⁶, C. Potterat³³, A. Powell⁵², J. Prisciandaro³⁶, V. Pugatch⁴¹, A. Puig Navarro³⁶,
 W. Qian⁴, J.H. Rademacker⁴³, B. Rakotomiaramanana³⁶, M.S. Rangel², I. Raniuk⁴⁰,
 N. Rauschmayr³⁵, G. Raven³⁹, S. Redford⁵², M.M. Reid⁴⁵, A.C. dos Reis¹, S. Ricciardi⁴⁶,
 A. Richards⁵⁰, K. Rinnert⁴⁹, V. Rives Molina³³, D.A. Roa Romero⁵, P. Robbe⁷,
 E. Rodrigues⁵¹, P. Rodriguez Perez³⁴, G.J. Rogers⁴⁴, S. Roiser³⁵, V. Romanovsky³²,
 A. Romero Vidal³⁴, J. Rouvinet³⁶, T. Ruf³⁵, H. Ruiz³³, G. Sabatino^{22,k}, J.J. Saborido Silva³⁴,
 N. Sagidova²⁷, P. Sail⁴⁸, B. Saitta^{15,d}, C. Salzmann³⁷, B. Sanmartin Sedes³⁴, M. Sannino^{19,i},
 R. Santacesaria²², C. Santamarina Rios³⁴, R. Santinelli³⁵, E. Santovetti^{21,k}, M. Sapunov⁶,
 A. Sarti^{18,l}, C. Satriano^{22,m}, A. Satta²¹, M. Savrie^{16,e}, D. Savrina^{28,29}, P. Schaack⁵⁰,
 M. Schiller³⁹, H. Schindler³⁵, S. Schleich⁹, M. Schlupp⁹, M. Schmelling¹⁰, B. Schmidt³⁵,
 O. Schneider³⁶, A. Schopper³⁵, M.-H. Schune⁷, R. Schwemmer³⁵, B. Sciascia¹⁸, A. Sciubba^{18,l},
 M. Seco³⁴, A. Semennikov²⁸, K. Senderowska²⁴, I. Sepp⁵⁰, N. Serra³⁷, J. Serrano⁶, P. Seyfert¹¹,
 M. Shapkin³², I. Shapoval^{35,40}, P. Shatalov²⁸, Y. Shcheglov²⁷, T. Shears^{49,35}, L. Shekhtman³¹,
 O. Shevchenko⁴⁰, V. Shevchenko²⁸, A. Shires⁵⁰, R. Silva Coutinho⁴⁵, T. Skwarnicki⁵³,
 N.A. Smith⁴⁹, E. Smith^{52,46}, M. Smith⁵¹, K. Sobczak⁵, F.J.P. Soler⁴⁸, F. Soomro¹⁸, D. Souza⁴³,

B. Souza De Paula², B. Spaan⁹, A. Sparkes⁴⁷, P. Spradlin⁴⁸, F. Stagni³⁵, S. Stahl¹¹, O. Steinkamp³⁷, S. Stoica²⁶, S. Stone⁵³, B. Storaci³⁷, M. Straticiuc²⁶, U. Straumann³⁷, V.K. Subbiah³⁵, S. Swientek⁹, V. Syropoulos³⁹, M. Szczekowski²⁵, P. Szczypka^{36,35}, T. Szumlak²⁴, S. T'Jampens⁴, M. Teklishyn⁷, E. Teodorescu²⁶, F. Teubert³⁵, C. Thomas⁵², E. Thomas³⁵, J. van Tilburg¹¹, V. Tisserand⁴, M. Tobin³⁷, S. Tolk³⁹, D. Tonelli³⁵, S. Topp-Joergensen⁵², N. Torr⁵², E. Tournefier^{4,50}, S. Tourneur³⁶, M.T. Tran³⁶, M. Tresch³⁷, A. Tsaregorodtsev⁶, P. Tsopelas³⁸, N. Tuning³⁸, M. Ubeda Garcia³⁵, A. Ukleja²⁵, D. Urner⁵¹, U. Uwer¹¹, V. Vagnoni¹⁴, G. Valenti¹⁴, R. Vazquez Gomez³³, P. Vazquez Regueiro³⁴, S. Vecchi¹⁶, J.J. Velthuis⁴³, M. Veltri^{17,g}, G. Veneziano³⁶, M. Vesterinen³⁵, B. Viaud⁷, I. Videau⁷, D. Vieira², X. Vilasis-Cardona^{33,n}, J. Visniakov³⁴, A. Vollhardt³⁷, D. Volyanskyy¹⁰, D. Voong⁴³, A. Vorobyev²⁷, V. Vorobyev³¹, C. Voß⁵⁵, H. Voss¹⁰, R. Waldi⁵⁵, R. Wallace¹², S. Wandernoth¹¹, J. Wang⁵³, D.R. Ward⁴⁴, N.K. Watson⁴², A.D. Webber⁵¹, D. Websdale⁵⁰, M. Whitehead⁴⁵, J. Wicht³⁵, D. Wiedner¹¹, L. Wiggers³⁸, G. Wilkinson⁵², M.P. Williams^{45,46}, M. Williams^{50,p}, F.F. Wilson⁴⁶, J. Wishahi⁹, M. Witek²³, W. Witzeling³⁵, S.A. Wotton⁴⁴, S. Wright⁴⁴, S. Wu³, K. Wyllie³⁵, Y. Xie^{47,35}, F. Xing⁵², Z. Xing⁵³, Z. Yang³, R. Young⁴⁷, X. Yuan³, O. Yushchenko³², M. Zangoli¹⁴, M. Zavertyaev^{10,a}, F. Zhang³, L. Zhang⁵³, W.C. Zhang¹², Y. Zhang³, A. Zhelezov¹¹, A. Zhokhov²⁸, L. Zhong³, A. Zvyagin³⁵.

¹ *Centro Brasileiro de Pesquisas Físicas (CBPF), Rio de Janeiro, Brazil*

² *Universidade Federal do Rio de Janeiro (UFRJ), Rio de Janeiro, Brazil*

³ *Center for High Energy Physics, Tsinghua University, Beijing, China*

⁴ *LAPP, Université de Savoie, CNRS/IN2P3, Annecy-Le-Vieux, France*

⁵ *Clermont Université, Université Blaise Pascal, CNRS/IN2P3, LPC, Clermont-Ferrand, France*

⁶ *CPPM, Aix-Marseille Université, CNRS/IN2P3, Marseille, France*

⁷ *LAL, Université Paris-Sud, CNRS/IN2P3, Orsay, France*

⁸ *LPNHE, Université Pierre et Marie Curie, Université Paris Diderot, CNRS/IN2P3, Paris, France*

⁹ *Fakultät Physik, Technische Universität Dortmund, Dortmund, Germany*

¹⁰ *Max-Planck-Institut für Kernphysik (MPIK), Heidelberg, Germany*

¹¹ *Physikalisches Institut, Ruprecht-Karls-Universität Heidelberg, Heidelberg, Germany*

¹² *School of Physics, University College Dublin, Dublin, Ireland*

¹³ *Sezione INFN di Bari, Bari, Italy*

¹⁴ *Sezione INFN di Bologna, Bologna, Italy*

¹⁵ *Sezione INFN di Cagliari, Cagliari, Italy*

¹⁶ *Sezione INFN di Ferrara, Ferrara, Italy*

¹⁷ *Sezione INFN di Firenze, Firenze, Italy*

¹⁸ *Laboratori Nazionali dell'INFN di Frascati, Frascati, Italy*

¹⁹ *Sezione INFN di Genova, Genova, Italy*

²⁰ *Sezione INFN di Milano Bicocca, Milano, Italy*

²¹ *Sezione INFN di Roma Tor Vergata, Roma, Italy*

²² *Sezione INFN di Roma La Sapienza, Roma, Italy*

²³ *Henryk Niewodniczanski Institute of Nuclear Physics Polish Academy of Sciences, Kraków, Poland*

²⁴ *AGH - University of Science and Technology, Faculty of Physics and Applied Computer Science, Kraków, Poland*

²⁵ *National Center for Nuclear Research (NCBJ), Warsaw, Poland*

²⁶ *Horia Hulubei National Institute of Physics and Nuclear Engineering, Bucharest-Magurele, Romania*

²⁷ *Petersburg Nuclear Physics Institute (PNPI), Gatchina, Russia*

²⁸ *Institute of Theoretical and Experimental Physics (ITEP), Moscow, Russia*

²⁹ *Institute of Nuclear Physics, Moscow State University (SINP MSU), Moscow, Russia*

³⁰ *Institute for Nuclear Research of the Russian Academy of Sciences (INR RAN), Moscow, Russia*

³¹ *Budker Institute of Nuclear Physics (SB RAS) and Novosibirsk State University, Novosibirsk, Russia*

- ³²*Institute for High Energy Physics (IHEP), Protvino, Russia*
³³*Universitat de Barcelona, Barcelona, Spain*
³⁴*Universidad de Santiago de Compostela, Santiago de Compostela, Spain*
³⁵*European Organization for Nuclear Research (CERN), Geneva, Switzerland*
³⁶*Ecole Polytechnique Fédérale de Lausanne (EPFL), Lausanne, Switzerland*
³⁷*Physik-Institut, Universität Zürich, Zürich, Switzerland*
³⁸*Nikhef National Institute for Subatomic Physics, Amsterdam, The Netherlands*
³⁹*Nikhef National Institute for Subatomic Physics and VU University Amsterdam, Amsterdam, The Netherlands*
⁴⁰*NSC Kharkiv Institute of Physics and Technology (NSC KIPT), Kharkiv, Ukraine*
⁴¹*Institute for Nuclear Research of the National Academy of Sciences (KINR), Kyiv, Ukraine*
⁴²*University of Birmingham, Birmingham, United Kingdom*
⁴³*H.H. Wills Physics Laboratory, University of Bristol, Bristol, United Kingdom*
⁴⁴*Cavendish Laboratory, University of Cambridge, Cambridge, United Kingdom*
⁴⁵*Department of Physics, University of Warwick, Coventry, United Kingdom*
⁴⁶*STFC Rutherford Appleton Laboratory, Didcot, United Kingdom*
⁴⁷*School of Physics and Astronomy, University of Edinburgh, Edinburgh, United Kingdom*
⁴⁸*School of Physics and Astronomy, University of Glasgow, Glasgow, United Kingdom*
⁴⁹*Oliver Lodge Laboratory, University of Liverpool, Liverpool, United Kingdom*
⁵⁰*Imperial College London, London, United Kingdom*
⁵¹*School of Physics and Astronomy, University of Manchester, Manchester, United Kingdom*
⁵²*Department of Physics, University of Oxford, Oxford, United Kingdom*
⁵³*Syracuse University, Syracuse, NY, United States*
⁵⁴*Pontifícia Universidade Católica do Rio de Janeiro (PUC-Rio), Rio de Janeiro, Brazil, associated to ²*
⁵⁵*Institut für Physik, Universität Rostock, Rostock, Germany, associated to ¹¹*

- ^a*P.N. Lebedev Physical Institute, Russian Academy of Science (LPI RAS), Moscow, Russia*
^b*Università di Bari, Bari, Italy*
^c*Università di Bologna, Bologna, Italy*
^d*Università di Cagliari, Cagliari, Italy*
^e*Università di Ferrara, Ferrara, Italy*
^f*Università di Firenze, Firenze, Italy*
^g*Università di Urbino, Urbino, Italy*
^h*Università di Modena e Reggio Emilia, Modena, Italy*
ⁱ*Università di Genova, Genova, Italy*
^j*Università di Milano Bicocca, Milano, Italy*
^k*Università di Roma Tor Vergata, Roma, Italy*
^l*Università di Roma La Sapienza, Roma, Italy*
^m*Università della Basilicata, Potenza, Italy*
ⁿ*LIFAELS, La Salle, Universitat Ramon Llull, Barcelona, Spain*
^o*Hanoi University of Science, Hanoi, Viet Nam*
^p*Massachusetts Institute of Technology, Cambridge, MA, United States*

Heavy quark effective theory (HQET) describes mesons with one heavy and one light quark where the heavy quark is assumed to have infinite mass [1]. It is an important tool for calculating meson properties which may be modified by physics beyond the Standard Model, such as CP violation in charm meson decays [2] or the mixing and lifetimes of B mesons [3]. It also predicts the properties of excited B and B_s^0 mesons [4–7], and precise measurements of these properties are a sensitive test of the validity of the theory. Within HQET the B_s^0 mesons are characterised by three quantum numbers: the relative orbital angular momentum L of the two quarks, the total angular momentum of the light quark $j_q = |L \pm \frac{1}{2}|$, and the total angular momentum of the B_s^0 meson $J = |j_q \pm \frac{1}{2}|$. For $L = 1$ there are four different possible (J, j_q) combinations, all with even parity. These are collectively termed the orbitally excited states. Such states can decay to B^+K^- and/or $B^{*+}K^-$ (the inclusion of charge-conjugate states is implied throughout this Letter), depending on their quantum numbers and mass values. The two states with $j_q = 1/2$, named B_{s0}^* and B_{s1}' , are expected to decay through an S-wave transition and to have a large $\mathcal{O}(100 \text{ MeV}/c^2)$ decay width. In contrast, the two states with $j_q = 3/2$, named $B_{s1}(5830)^0$ and $B_{s2}^*(5840)^0$ (henceforth B_{s1} and B_{s2}^* for brevity), are expected to decay through a D-wave transition and to have a narrow $\mathcal{O}(1 \text{ MeV}/c^2)$ decay width. Table 1 gives an overview of these states.

Table 1: Summary of the orbitally excited ($L = 1$) B_s^0 states.

	j_q	J^P	Allowed decay mode		Mass (MeV/ c^2) [8]
			B^+K^-	$B^{*+}K^-$	
B_{s0}^*	1/2	0^+	yes	no	Unobserved
B_{s1}'	1/2	1^+	no	yes	Unobserved
B_{s1}	3/2	1^+	no	yes	5829.4 ± 0.7
B_{s2}^*	3/2	2^+	yes	yes	5839.7 ± 0.6

In this Letter a 1.0 fb^{-1} sample of data collected by the LHCb detector is used to search for the orbitally excited B_s^0 mesons in the mass distribution of B^+K^- pairs, where the B^+ mesons are selected in the four decay modes: $B^+ \rightarrow J/\psi(\mu^+\mu^-)K^+$, $B^+ \rightarrow \bar{D}^0(K^+\pi^-)\pi^+$, $B^+ \rightarrow \bar{D}^0(K^+\pi^-\pi^+\pi^-)\pi^+$, and $B^+ \rightarrow \bar{D}^0(K^+\pi^-)\pi^+\pi^-\pi^+$. Two narrow peaks were observed in the B^+K^- mass distribution by the CDF collaboration [9]. Putatively, they are identified with the states of the $j_q = 3/2$ doublet expected in HQET [4] and are named B_{s1} and B_{s2}^* . As the $B_{s1} \rightarrow B^+K^-$ decay is forbidden, one of the mass peaks observed is interpreted as the $B_{s1} \rightarrow B^{*+}K^-$ decay followed by $B^{*+} \rightarrow B^+\gamma$, where the photon is not observed. This peak is shifted by the $B^{*+} - B^+$ mass difference due to the missing momentum of the photon in the $B^{*+} \rightarrow B^+\gamma$ decay. While the $B_{s2}^* \rightarrow B^+K^-$ decay has been observed by the D0 collaboration as well [10], a confirmation of the B_{s1} meson is still missing. The identification of the B_{s1} and B_{s2}^* mesons in the B^+K^- mass spectrum is based on the expected mass splitting between the $j_q = 3/2$ states. The B_{s1} and B_{s2}^* widths are very sensitive to their masses, due to their proximity to the BK and B^*K thresholds. Measurements of the widths thus provide fundamental information

concerning the nature of these states. In addition the B_{s1} and B_{s2}^* quantum numbers have not yet been directly determined and the observation of other decay modes can constrain the spin-parity combinations of the states. In particular the $B_{s2}^* \rightarrow B^{*+}K^-$ decay has not yet been observed but could manifest itself in the B^+K^- mass spectrum in a similar fashion to the corresponding B_{s1} meson decay. The $B_{s2}^* \rightarrow B^{*+}K^-$ branching fraction relative to $B_{s2}^* \rightarrow B^+K^-$ is predicted to be between 2% and 10%, depending on the B_{s2}^* mass [11–14].

Recently the Belle collaboration has reported observation of charged bottomonium-like $Z_b(10610)^+$ and $Z_b(10650)^+$ states [15, 16], that could be interpreted as $B\bar{B}^*$ and $B^*\bar{B}^*$ molecules respectively [17]. To test this interpretation, improved measurements of the B^{*+} mass are necessary, and can be obtained from the difference in peak positions between $B_{s2}^* \rightarrow B^{*+}K^-$ and $B_{s2}^* \rightarrow B^+K^-$ decays in the B^+K^- mass spectrum.

The LHCb detector [18] is a single-arm forward spectrometer covering the pseudorapidity range $2 < \eta < 5$, designed for studying particles containing b or c quarks. The detector includes a high-precision tracking system consisting of a silicon-strip vertex detector surrounding the pp interaction region, a large-area silicon-strip detector located upstream of a dipole magnet with a bending power of about 4 Tm, and three stations of silicon-strip detectors and straw drift tubes placed downstream. The combined tracking system has a momentum resolution $(\Delta p/p)$, that varies from 0.4% at 5 GeV/ c to 0.6% at 100 GeV/ c , and a decay time resolution of 50 fs. The resolution of the impact parameter, the transverse distance of closest approach between the track and a primary interaction, is about 20 μm for tracks with large transverse momentum. The transverse component is measured in the plane normal to the beam axis. Charged hadrons are identified using two ring-imaging Cherenkov detectors. Photon, electron and hadron candidates are identified by a calorimeter system consisting of scintillating-pad and pre-shower detectors, an electromagnetic calorimeter, and a hadronic calorimeter. Muons are identified by a system composed of alternating layers of iron and multiwire proportional chambers.

The trigger system [19] consists of a hardware stage, based on information from the calorimeter and muon systems, followed by a software stage that applies a full event reconstruction. Events likely to contain a B meson are selected by searching for a dimuon vertex detached from the primary interaction or two-, three-, and four-track vertices detached from the primary interaction which have high total transverse momentum. These are respectively referred to as dimuon and topological triggers.

The samples of simulated events used in this analysis are based on the PYTHIA 6.4 generator [20], with a choice of parameters specifically configured for LHCb [21]. The EVTGEN package [22] describes the decay of the B mesons, and the GEANT4 toolkit [23, 24] is used to simulate the detector response. QED radiative corrections are generated with the PHOTOS package [25].

In the offline analysis the B mesons are reconstructed using a set of loose selection criteria to suppress the majority of the combinatorial backgrounds. The $B^+ \rightarrow J/\psi K^+$ selection requires a B^+ candidate with a transverse momentum of at least 2 GeV/ c and a decay time of at least 0.3 ps. For the other decay modes, the selection explicitly requires that the topological trigger, which selected the event, is based exclusively on tracks from

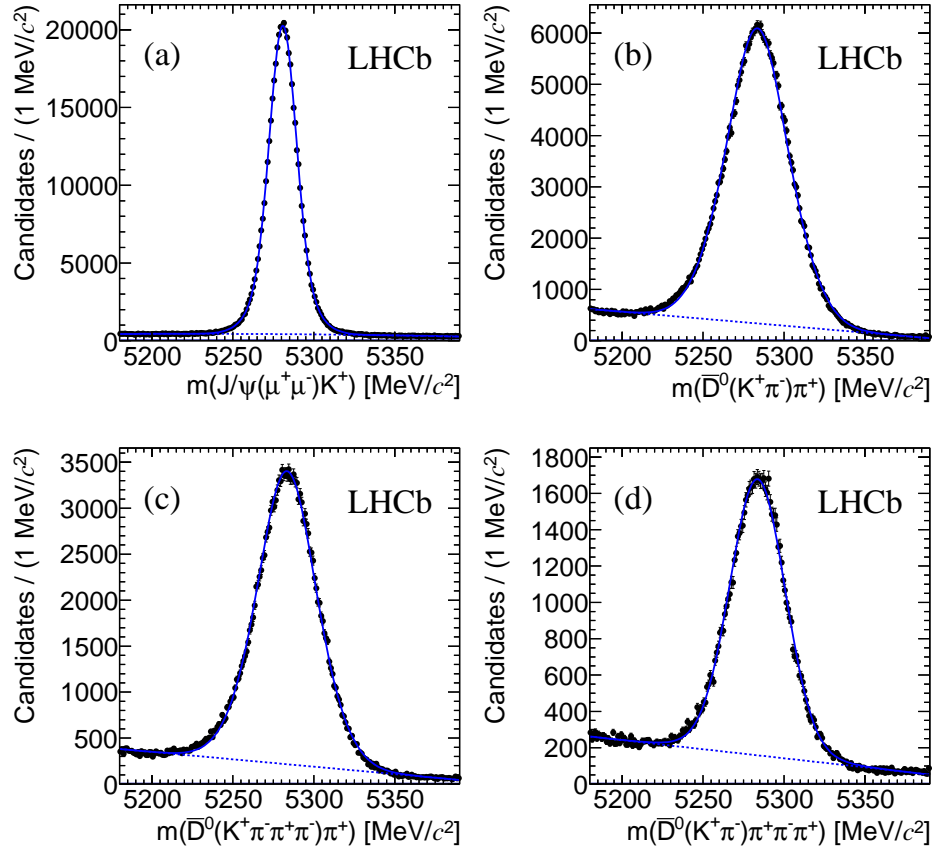


Figure 1: Invariant mass spectra of the final B^+ candidates. The signal lineshape is fitted with a double Gaussian distribution, while the background is modelled with a second order polynomial. (a) $B^+ \rightarrow J/\psi K^+$, (b) $B^+ \rightarrow \bar{D}^0(K^+\pi^-)\pi^+$, (c) $B^+ \rightarrow \bar{D}^0(K^+\pi^-\pi^+\pi^-)\pi^+$, and (d) $B^+ \rightarrow \bar{D}^0(K^+\pi^-)\pi^+\pi^-\pi^+$ decays. The J/ψ and D^0 masses are constrained to their world average values.

which the B meson candidate is formed. Additional loose selection requirements are placed on variables related to the B meson production and decay such as transverse momentum and quality of the track fits for the decay products, detachment of the B^+ candidate from the primary interaction, whether the momentum of the B^+ candidate points back to the primary interaction, and the impact parameter χ^2 . The impact parameter χ^2 is defined as the difference between the χ^2 of the primary vertex reconstructed with and without the considered track.

Following these selections, B^+ signals are visible above backgrounds in all four decay modes. In order to improve their purity, four boosted decision tree classifiers [26] are trained on variables common to all four decay modes: the transverse momenta and impact parameters of the final state tracks, the transverse momentum and impact parameter of the B^+ candidate, the detachment of the B^+ candidate from the primary interaction, the cosine of the angle between the B^+ candidate momentum and the direction of flight from

the primary vertex to the decay vertex, the fit χ^2 of the tracks, and particle identification information. The classifier is trained on data using the *sWeights* technique [27], with the B^+ candidate mass as a discriminating variable, to unfold the signal and background distributions. The cut on the classifier response is chosen by optimizing the significance of each B^+ signal. The final mass distributions for the B^+ candidates are shown in Fig. 1.

The B^+ candidate mass spectra are fitted using a double Gaussian function for the signal and a second order polynomial for the background. The average mass resolution, σ_{B^+} , is defined as the weighted average of the Gaussian widths. The purities of the samples, defined as the fraction of the signal events in a $\pm 2\sigma_{B^+}$ mass region, are 96%, 91%, 90%, and 85% for the $B^+ \rightarrow J/\psi K^+$, $B^+ \rightarrow \bar{D}^0(K^+\pi^-)\pi^+$, $B^+ \rightarrow \bar{D}^0(K^+\pi^-\pi^+\pi^-)\pi^+$, and $B^+ \rightarrow \bar{D}^0(K^+\pi^-)\pi^+\pi^-\pi^+$ decays respectively. The B^+ candidates, within a $\pm 2\sigma_{B^+}$ mass region, are selected for each decay mode. A sample of about 1 000 000 B^+ candidates is obtained and combined with any track of opposite charge that is identified as a kaon.

Multiple pp interactions can occur in LHC bunch crossings. In order to reduce combinatorial backgrounds, the B^+ and kaon candidates are required to be consistent with coming from the same interaction point. The signal purity is improved by a boosted decision tree classifier, whose inputs are the B^+ and the kaon transverse momenta, the log-likelihood difference between the kaon and pion hypotheses, and the vertex fit and impact parameter χ^2 . The training is performed using simulated events for the signal and the like-charge B^+K^+ candidates in the data for the background. The same selection is subsequently applied to all B^+ decay modes. The cut on the classifier response is chosen by optimizing the significance of the $B_{s2}^* \rightarrow B^+K^-$ signal. It retains 57% of the signal events and rejects 92% of the background events. In order to improve the mass resolution, the B^+K^- mass fits are performed constraining the J/ψ (or D^0) and B^+ particles to their respective world average masses [8] and constraining the B^+ and K^- momenta to point to the associated primary vertex.

Figure 2 shows the mass difference for the selected candidates, summed over all B^+ decay modes. The mass difference is defined as $Q \equiv m(B^+K^-) - m(B^+) - m(K^-)$ where $m(B^+)$ and $m(K^-)$ are the known masses of the B^+ and K^- mesons [8], respectively. The two narrow peaks at 10 and 67 MeV/ c^2 are identified as the $B_{s1} \rightarrow B^{*+}K^-$ and $B_{s2}^* \rightarrow B^+K^-$ signals, respectively, as previously observed. In addition, a smaller structure is seen around 20 MeV/ c^2 , identified as the previously unobserved $B_{s2}^* \rightarrow B^{*+}K^-$ decay mode.

Simulated events are used to compute the detector resolutions corresponding to the three signals. The values obtained are increased by 20% to account for differences between the B^+ resolutions in data and simulated events. The corrected resolutions are 0.4 MeV/ c^2 , 0.6 MeV/ c^2 and 1.0 MeV/ c^2 for the $B_{s1} \rightarrow B^{*+}K^-$, $B_{s2}^* \rightarrow B^{*+}K^-$, and $B_{s2}^* \rightarrow B^+K^-$ signals respectively. A discrepancy of 40% between the mass resolutions in data and simulated events is observed for decays with small Q values, such as $D^{*+} \rightarrow D^0\pi^+$. Therefore we assign an uncertainty of $\pm 20\%$ to the resolution in the systematic studies.

An unbinned fit of the mass difference distribution is performed to extract the Q values and event yields of the three peaks. The $B_{s2}^* \rightarrow B^+K^-$ signal is parameterized by a relativistic Breit-Wigner function with natural width Γ convolved with a Gaussian

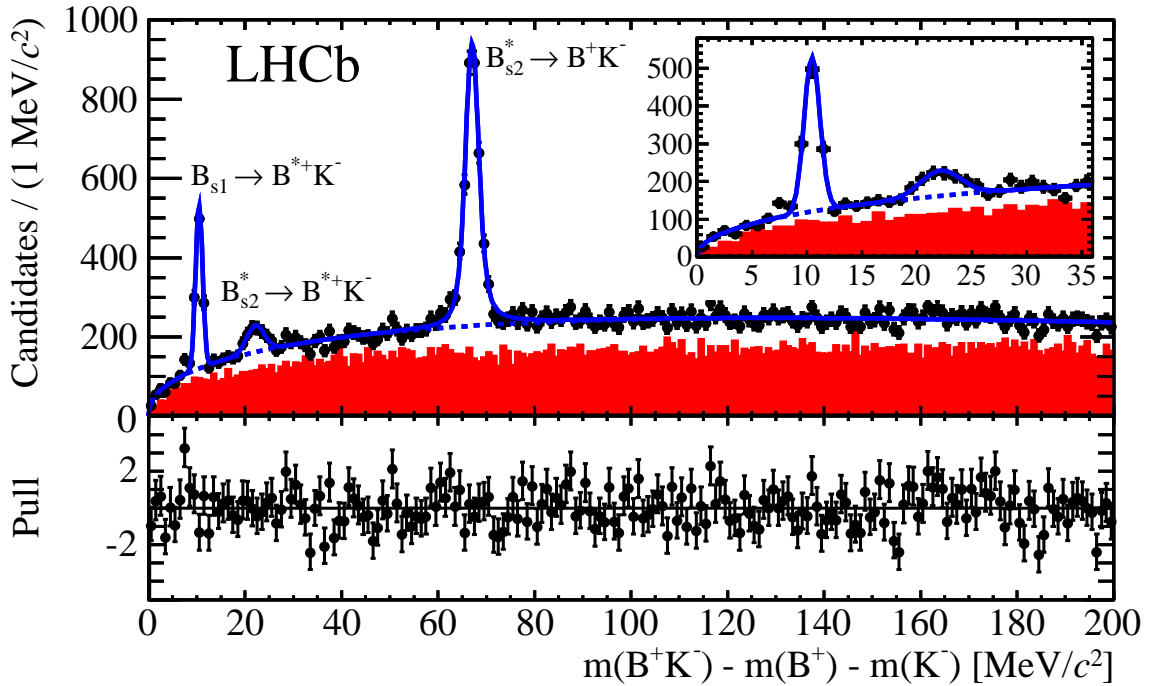


Figure 2: Mass difference distribution $m(B^+K^-) - m(B^+) - m(K^-)$. The three peaks are identified as (left) $B_{s1} \rightarrow B^{*+}K^-$, (middle) $B_{s2}^* \rightarrow B^{*+}K^-$, and (right) $B_{s2}^* \rightarrow B^+K^-$. The total fit function is shown as a solid blue line, while the shaded red region is the spectrum of like-charge B^+K^+ combinations. The inset shows an expanded view of the $B_{s1}/B_{s2}^* \rightarrow B^{*+}K^-$ signals. The bottom plot shows the fit pulls.

function that accounts for the detector resolution. Its width is fixed to the value obtained from simulated events. The lineshapes of the $B_{s1}/B_{s2}^* \rightarrow B^{*+}K^-$ signals, expected to be Breit-Wigner functions in the $B^{*+}K^-$ mass spectrum, are affected by the phase space and the angular distribution of the decays as the photon is not reconstructed. The resulting shapes can not be properly simulated due to the lack of knowledge of the B_{s1}/B_{s2}^* properties. Therefore a Gaussian function is used for each $B_{s1}/B_{s2}^* \rightarrow B^{*+}K^-$ signals as effective parameterization. The background is modelled by a threshold function, $f(Q) = Q^\alpha e^{\beta Q + \delta}$, where α , β and δ are free parameters in the fit. Its analytical form is verified by fitting the like charge B^+K^+ combinations where no signal is expected.

The parameters allowed to vary in the fit are: the yield $N_{B_{s2}^* \rightarrow B^+K^-}$, the yield ratios $N_{B_{s1} \rightarrow B^{*+}K^-}/N_{B_{s2}^* \rightarrow B^+K^-}$ and $N_{B_{s2}^* \rightarrow B^{*+}K^-}/N_{B_{s2}^* \rightarrow B^+K^-}$, the Q values of the $B_{s1} \rightarrow B^{*+}K^-$ and $B_{s2}^* \rightarrow B^+K^-$ signals, the mass difference between the $B_{s2}^* \rightarrow B^+K^-$ and $B_{s2}^* \rightarrow B^{*+}K^-$ peaks, the natural width of the B_{s2}^* state, the Gaussian widths of $B_{s1}/B_{s2}^* \rightarrow B^{*+}K^-$ signals and the parameters of the threshold function. From the yield ratios, the relative branching fraction

$$\frac{\mathcal{B}(B_{s2}^* \rightarrow B^{*+}K^-)}{\mathcal{B}(B_{s2}^* \rightarrow B^+K^-)} = \frac{N_{B_{s2}^* \rightarrow B^{*+}K^-}}{N_{B_{s2}^* \rightarrow B^+K^-}} \times \epsilon_{2,2}^{\text{rel}} = R^{B_{s2}^*} \quad (1)$$

Table 2: Results of the fit to the mass difference distributions $m(B^+K^-) - m(B^+) - m(K^-)$. The first uncertainties are statistical and the second are systematic.

Parameter	Fit result	Best previous measurement
$m(B_{s1}) - m(B^{*+}) - m(K^-)$	$10.46 \pm 0.04 \pm 0.04 \text{ MeV}/c^2$	$10.73 \pm 0.21 \pm 0.14 \text{ MeV}/c^2$ [9]
$m(B_{s2}^*) - m(B^+) - m(K^-)$	$67.06 \pm 0.05 \pm 0.11 \text{ MeV}/c^2$	$66.96 \pm 0.39 \pm 0.14 \text{ MeV}/c^2$ [9]
$m(B^{*+}) - m(B^+)$	$45.01 \pm 0.30 \pm 0.23 \text{ MeV}/c^2$	$45.6 \pm 0.8 \text{ MeV}/c^2$ [28]
$\Gamma(B_{s2}^*)$	$1.56 \pm 0.13 \pm 0.47 \text{ MeV}/c^2$	
$\frac{\mathcal{B}(B_{s2}^* \rightarrow B^{*+}K^-)}{\mathcal{B}(B_{s2}^* \rightarrow B^+K^-)}$	$(9.3 \pm 1.3 \pm 1.2) \%$	
$\frac{\sigma(pp \rightarrow B_{s1}X)\mathcal{B}(B_{s1} \rightarrow B^{*+}K^-)}{\sigma(pp \rightarrow B_{s2}^*X)\mathcal{B}(B_{s2}^* \rightarrow B^+K^-)}$	$(23.2 \pm 1.4 \pm 1.3) \%$	
$N_{B_{s1} \rightarrow B^{*+}K^-}$	750 ± 36	
$N_{B_{s2}^* \rightarrow B^{*+}K^-}$	307 ± 46	
$N_{B_{s2}^* \rightarrow B^+K^-}$	3140 ± 100	

is measured. The B_{s1} to B_{s2}^* ratio of production cross-sections times the ratio of branching fractions of $B_{s1} \rightarrow B^{*+}K^-$ relative to that of $B_{s2}^* \rightarrow B^+K^-$ is also determined from

$$\frac{\sigma(pp \rightarrow B_{s1}X)\mathcal{B}(B_{s1} \rightarrow B^{*+}K^-)}{\sigma(pp \rightarrow B_{s2}^*X)\mathcal{B}(B_{s2}^* \rightarrow B^+K^-)} = \frac{N_{B_{s1} \rightarrow B^{*+}K^-}}{N_{B_{s2}^* \rightarrow B^+K^-}} \times \epsilon_{1,2}^{\text{rel}} = \sigma^{B_{s1}/B_{s2}^*} R^{B_{s1}/B_{s2}^*} \quad (2)$$

These ratios are corrected by the relative selection efficiencies, $\epsilon_{2,2}^{\text{rel}} = 1.05 \pm 0.02$ and $\epsilon_{1,2}^{\text{rel}} = 1.03 \pm 0.01$, using simulated decays. The fit results are given in Table 2. The widths of the two Gaussian functions are $0.73 \pm 0.04 \text{ MeV}/c^2$ and $1.9 \pm 0.3 \text{ MeV}/c^2$ for the $B_{s1} \rightarrow B^{*+}K^-$ and $B_{s2}^* \rightarrow B^{*+}K^-$ signals respectively. A binned χ^2 test gives a confidence level of 43% for the fit.

To determine the significance of the $B_{s2}^* \rightarrow B^{*+}K^-$ signal, a similar maximum likelihood fit is performed, where all parameters of the signal are fixed according to expectation, except its yield. The likelihood of this fit is compared to the result of a fit where the yield of the signal is fixed to zero. The statistical significance of the $B_{s2}^* \rightarrow B^{*+}K^-$ signal is 8σ .

A number of systematic uncertainties are considered. For the signal model, the signal shape is changed to a double Gaussian function and an alternative threshold function is used for the background. The changes in the fit results are assigned as the associated uncertainties. The B^+ decay modes are fitted independently to test for effects that may be related to differences in their selection requirements. For each observable quoted in Table 2, the difference between the weighted average of these independent fits and the global fit is taken as a systematic uncertainty. Additional systematic uncertainties are assigned based on the change in the results when varying the selection criteria and the B^+ signal region. The detector resolution of $B_{s2}^* \rightarrow B^+K^-$ signal is varied by $\pm 20\%$. In addition, the momentum scale in the processing of the data used in this analysis is varied within the estimated uncertainty of 0.15%. The corresponding uncertainty on

Table 3: Absolute systematic uncertainties for each measurement, which are assumed to be independent and are added in quadrature.

Source	$Q(B_{s1})$ (MeV/ c^2)	$Q(B_{s2}^*)$ (MeV/ c^2)	$m(B^{*+}) - m(B^+)$ (MeV/ c^2)	$\Gamma(B_{s2}^*)$ (MeV/ c^2)	$R^{B_{s2}^*}$ (%)	$\sigma^{B_{s1}/B_{s2}^*} R^{B_{s1}/B_{s2}^*}$ (%)
Fit model	0.00	0.02	0.03	0.01	0.2	0.5
B^+ decay mode	0.01	0.01	0.02	0.01	0.1	0.1
Selection	0.03	0.02	0.19	0.05	1.1	0.6
B^+ signal region	0.01	0.03	0.11	0.07	0.2	0.4
Mass resolution	0.00	0.01	0.02	0.46	0.2	0.9
Momentum scale	0.02	0.10	0.03	-	-	-
Efficiency ratios	-	-	-	-	0.2	0.2
Missing photon	0.01	-	0.01	-	-	-
Total	0.04	0.11	0.23	0.47	1.2	1.3

the measured masses is assigned as a systematic uncertainty. The uncertainty on the determination of the selection efficiency ratios caused by finite samples of simulated events is taken as a systematic uncertainty for the branching fractions. Finally simulated events are used to estimate the mass shifts of the $B_{s1}/B_{s2}^* \rightarrow B^{*+}K^-$ signals from the nominal values when the radiated photon is excluded from their reconstructed decays. The absolute systematic uncertainties are given in Table 3. The $B_{s2}^* \rightarrow B^{*+}K^-$ signal is observed with the expected frequency in each of the four reconstructed decay modes and the systematic error for the $\frac{\mathcal{B}(B_{s2}^* \rightarrow B^{*+}K^-)}{\mathcal{B}(B_{s2}^* \rightarrow B^+K^-)}$ branching fraction ratio, related to the different B^+ decay modes, is small. The final results are shown in Table 2. The measured mass differences are more precise than the previous best measurements of a factor two at least. The measured $\frac{\mathcal{B}(B_{s2}^* \rightarrow B^{*+}K^-)}{\mathcal{B}(B_{s2}^* \rightarrow B^+K^-)}$ branching fraction ratio and B_{s2}^* width are in good agreement with theoretical predictions [12–14].

The mass differences given in Table 2 are translated into absolute masses by adding the masses of the B^+ and kaon [8] and, in the case of the B_{s1} meson, the $B^{*+} - B^+$ mass difference measured in this Letter. The results are

$$\begin{aligned} m(B^{*+}) &= 5324.26 \pm 0.30 \pm 0.23 \pm 0.17 \text{ MeV}/c^2, \\ m(B_{s1}) &= 5828.40 \pm 0.04 \pm 0.04 \pm 0.41 \text{ MeV}/c^2, \\ m(B_{s2}^*) &= 5839.99 \pm 0.05 \pm 0.11 \pm 0.17 \text{ MeV}/c^2, \end{aligned}$$

where the first uncertainty is statistical and the second is systematic. The third uncertainty corresponds to the uncertainty on the B^+ mass [8] and, in the case of the B_{s1} mass measurement, the uncertainty on the $B^{*+} - B^+$ mass difference measured in this analysis.

The significance of the non-zero B_{s2}^* width is determined by comparing the likelihood for the nominal fit with a fit in which the width is fixed to zero. To account for systematic effects, the minimum $\sqrt{2\Delta\log\mathcal{L}}$ among all systematic variations is taken; the significance including systematic uncertainties is 9σ .

In conclusion, using 1.0 fb^{-1} of data collected with the LHCb detector at $\sqrt{s} = 7 \text{ TeV}$, the decay mode $B_{s2}^* \rightarrow B^{*+}K^-$ is observed for the first time and its branching fraction

measured relative to that of $B_{s2}^* \rightarrow B^+ K^-$. The observation of the B_{s2}^* meson decaying to two pseudoscalars ($B_{s2}^* \rightarrow B^+ K^-$) and to a vector and a pseudoscalar ($B_{s2}^* \rightarrow B^{*+} K^-$) favours the assignment of $J^P = 2^+$ for this state. The B_{s2}^* width is measured for the first time, while the masses of the B_{s1} and B_{s2}^* states are measured with the highest precision to date and are consistent with previous measurements [9, 10]. Finally, the observed $B_{s2}^* \rightarrow B^{*+} K^-$ decay is used to make the most precise measurement to date of the $B^{*+} - B^+$ mass difference. This measurement, unlike others reported in the literature, does not require the reconstruction of the soft photon from B^{*+} decays and therefore has significantly smaller systematic uncertainty. High precision measurements of the B^{*+} mass are important for the understanding of the exotic Z_b^+ states recently observed [15]. Using the B^{*+} mass measured in this analysis, we compute that the $Z_b(10610)^+$ and $Z_b(10650)^+$ masses are $3.69 \pm 2.05 \text{ MeV}/c^2$ and $3.68 \pm 1.71 \text{ MeV}/c^2$ above the $B\bar{B}^*$ and $B^*\bar{B}^*$ thresholds respectively.

Acknowledgements

We express our gratitude to our colleagues in the CERN accelerator departments for the excellent performance of the LHC. We thank the technical and administrative staff at the LHCb institutes. We acknowledge support from CERN and from the national agencies: CAPES, CNPq, FAPERJ and FINEP (Brazil); NSFC (China); CNRS/IN2P3 and Region Auvergne (France); BMBF, DFG, HGF and MPG (Germany); SFI (Ireland); INFN (Italy); FOM and NWO (The Netherlands); SCSR (Poland); ANCS/IFA (Romania); MinES, Rosatom, RFBR and NRC ‘‘Kurchatov Institute’’ (Russia); MinECo, XuntaGal and GENCAT (Spain); SNSF and SER (Switzerland); NAS Ukraine (Ukraine); STFC (United Kingdom); NSF (USA). We also acknowledge the support received from the ERC under FP7. The Tier1 computing centres are supported by IN2P3 (France), KIT and BMBF (Germany), INFN (Italy), NWO and SURF (The Netherlands), PIC (Spain), GridPP (United Kingdom). We are thankful for the computing resources put at our disposal by Yandex LLC (Russia), as well as to the communities behind the multiple open source software packages that we depend on.

References

- [1] T. Mannel, *Review of heavy quark effective theory*, [arXiv:hep-ph/9611411](#).
- [2] M. Bobrowski, A. Lenz, J. Riedl, and J. Rohrwild, *How large can the SM contribution to CP violation in $D^0 - \bar{D}^0$ mixing be?*, *JHEP* **03** (2010) 009, [arXiv:1002.4794](#).
- [3] A. Lenz, *Theoretical update of B-mixing and lifetimes*, [arXiv:1205.1444](#).
- [4] M. Di Pierro and E. Eichten, *Excited heavy-light systems and hadronic transitions*, *Phys. Rev.* **D64** (2001) 114004, [arXiv:hep-ph/0104208](#).

- [5] E. J. Eichten, C. T. Hill, and C. Quigg, *Properties of orbitally excited heavy-light ($Q\bar{q}$) mesons*, Phys. Rev. Lett. **71** (1993) 4116, arXiv:hep-ph/9308337.
- [6] A. F. Falk and T. Mehen, *Excited heavy mesons beyond leading order in the heavy quark expansion*, Phys. Rev. **D53** (1996) 231, arXiv:hep-ph/9507311.
- [7] UKQCD collaboration, J. Koponen, *Energies of B_s meson excited states: a lattice study*, Phys. Rev. **D78** (2008) 074509, arXiv:0708.2807.
- [8] Particle Data Group, J. Beringer *et al.*, *Review of particle physics*, Phys. Rev. **D86** (2012) 010001.
- [9] CDF collaboration, T. Aaltonen *et al.*, *Observation of orbitally excited B_s mesons*, Phys. Rev. Lett. **100** (2008) 082001, arXiv:0710.4199.
- [10] D0 collaboration, V. Abazov *et al.*, *Observation and properties of the orbitally excited B_{s2}^* meson*, Phys. Rev. Lett. **100** (2008) 082002, arXiv:0711.0319.
- [11] S. Godfrey and R. Kokoski, *The properties of P-wave mesons with one heavy quark*, Phys. Rev. **D43** (1991) 1679.
- [12] P. Colangelo, F. De Fazio, F. Giannuzzi, and S. Nicotri, *New meson spectroscopy with open charm and beauty*, Phys. Rev. **D86** (2012) 054024, arXiv:1207.6940.
- [13] X.-H. Zhong and Q. Zhao, *Strong decays of heavy-light mesons in a chiral quark model*, Phys. Rev. **D78** (2008) 014029, arXiv:0803.2102.
- [14] Z.-H. Wang, G.-L. Wang, H.-F. Fu, and Y. Jiang, *The strong decays of orbitally excited B_{sJ}^* mesons by improved Bethe-Salpeter method*, Phys. Lett. **B706** (2012) 389, arXiv:1202.1224.
- [15] Belle collaboration, A. Bondar *et al.*, *Observation of two charged bottomonium-like resonances in $\Upsilon(5S)$ decays*, Phys. Rev. Lett. **108** (2012) 122001, arXiv:1110.2251.
- [16] Belle collaboration, I. Adachi *et al.*, *Study of three-body $\Upsilon(10860)$ decays*, arXiv:1209.6450.
- [17] A. Bondar *et al.*, *Heavy quark spin structure in Z_b resonances*, Phys. Rev. **D84** (2011) 054010, arXiv:1105.4473.
- [18] LHCb collaboration, A. A. Alves Jr. *et al.*, *The LHCb detector at the LHC*, JINST **3** (2008) S08005.
- [19] R. Aaij *et al.*, *The LHCb trigger and its performance*, arXiv:1211.3055.
- [20] T. Sjöstrand, S. Mrenna, and P. Skands, *PYTHIA 6.4 physics and manual*, JHEP **05** (2006) 026, arXiv:hep-ph/0603175.

- [21] I. Belyaev *et al.*, *Handling of the generation of primary events in GAUSS, the LHCb simulation framework*, Nuclear Science Symposium Conference Record (NSS/MIC) **IEEE** (2010) 1155.
- [22] D. J. Lange, *The EvtGen particle decay simulation package*, Nucl. Instrum. Meth. **A462** (2001) 152.
- [23] GEANT4 collaboration, J. Allison *et al.*, *Geant4 developments and applications*, IEEE Trans. Nucl. Sci. **53** (2006) 270; GEANT4 collaboration, S. Agostinelli *et al.*, *GEANT4: A simulation toolkit*, Nucl. Instrum. Meth. **A506** (2003) 250.
- [24] M. Clemencic *et al.*, *The LHCb simulation application, GAUSS: design, evolution and experience*, J. of Phys. : Conf. Ser. **331** (2011) 032023.
- [25] P. Golonka and Z. Was, *PHOTOS Monte Carlo: A precision tool for QED corrections in Z and W decays*, Eur. Phys. J. **C45** (2006) 97, arXiv:hep-ph/0506026.
- [26] L. Breiman, J. H. Friedman, R. A. Olshen, and C. J. Stone, *Classification and regression trees*, Wadsworth international group, Belmont, California, USA, 1984; B. P. Roe *et al.*, *Boosted decision trees as an alternative to artificial neural networks for particle identification*, Nucl. Instrum. Meth. **A543** (2005) 577, arXiv:physics/0408124.
- [27] M. Pivk and F. R. Le Diberder, *SPlot: A statistical tool to unfold data distributions*, Nucl. Instrum. Meth. **A555** (2005) 356, arXiv:physics/0402083.
- [28] Q. Wu *et al.*, *Measurement of the B^* cross-section at $\sqrt{s} = 10.61$ to 10.70 GeV*, Phys. Lett. **B273** (1991) 177.